Accepted for publication in *Journal of Membrane Science* (**2025**)

Microporous Pentiptycene-based Polybenzimidazole Membranes for High Temperature H_2/CO_2 Separation

Mengdi Liu, Joseph Emery, and Ruilan Guo*

Department of Chemical and Biomolecular Engineering, University of Notre Dame

Indiana, 46556, United States

* Corresponding author. Email: rguo@nd.edu

Abstract: Separating H_2 from syngas at elevated temperatures (100-250 ºC) have attracted significant attention in recent years as a means to reduce energy consumption and capital costs in precombustion carbon capture processes, such as those following steam reforming of natural gas or coal gasification. Polybenzimidazole (PBI), particularly *m*-PBI, has been reported as a leading membrane material for high-temperature H_2/CO_2 separation. However, *m*-PBI exhibits extremely low H_2 permeability, even at high temperatures, which limits its productivity in H_2/CO_2 separation applications. To address this limitation, this work introduces a new pentiptycene-based polybenzimidazole (PPBI) featuring significantly enhanced H_2 permeability and attractive high-temperature H_2/CO_2 separation performance, which stems from the unique configurational free volume elements introduced by pentiptycene moieties. Further tuning of the free volume architecture of PPBI films is achieved via acid doping with phosphoric acid (PA) or trans-aconitic acid (TaA), which introduces crosslinking among PPBI chains. Under mixed-gas environment (50/50 mol% H_2/CO_2) at 180 ºC, the acid-doped PPBI films exhibit a ~230% increase in H_2/CO_2 selectivity compared to pristine PPBI film while maintaining high H_2 permeability that is nearly 500% of *m*-PBI. These properties approach the predicted upper bound for membrane operating at 180 ºC, highlighting its great potential for high-temperature H_2/CO_2 separation.

1. Introduction

Chemical separations consume about 17,000 quadrillion Joule of energy per year in the United States, which approximates 50% of all in-plant energy use.[1] Membrane-assisted separation technology represents an alternative energy-efficient technology that is environmentally friendly with low carbon footprint and simple operation, as it doesn't involve potentially toxic media or rely on intensive thermal energy required by existing separation technologies, such as distillation and adsorption.[2] As one of clean energy sources, the market of hydrogen (H_2) production has grown rapidly in recent decades.[3-5] Currently, H_2 is predominately (>90%) produced as syngas via steam reforming of natural gas or coal gasification after the water-gas shift reaction[6, 7], generating ~55% H_2 and ~40% CO_2 at 200-300 ºC and 20-40 bar.[8-10] Separating CO_2 from H_2, also known as pre-combustion carbon capture, is a critical process to mitigate CO_2 emissions to the atmosphere while producing high-purity H_2 fuels.[10, 11] Current leading technologies for pre-combustion CO_2 capture are absorption processes involving toxic and corrosive absorbents (i.e., Selexol® and Rectisol®), which also demand considerable amount of energy and high capital costs due to the complex absorber-stripper operation and recompression of CO_2.[12] Therefore, high-performance membranes for H_2/CO_2 separation are highly desirable as a more environmentally friendly and energy-efficient approach to produce clean H_2 fuels as well as sequestrate CO_2.

Polybenzimidazole (PBI), such as *m*-PBI (Celazole®), is the leading membrane material for H_2/CO_2 separation due to its outstanding thermal stability and excellent size-sieving property.[13] However, *m*-PBI suffers from extremely low gas permeability that limits its industry applications. Although many previous studies have attempted to improve PBI's permeability by incorporating bulky sulfone bridges,[14, 15] bulky fluorinated groups[13, 16-18], or blending *m*-PBI with other highly permeable polymers[19-21], these strategies typically resulted in compromised size-sieving capability,

particularly at high temperatures (e.g., 150-200 ºC), due to transient gas transport pathways constructed by polymer free volume microvoids with random and broad size distribution.[22, 23] At elevated temperatures, increased segmental mobility of polymer chains promotes chain relaxation and the potential extension of conformational free volume elements, which typically results in more obviously enhanced diffusion of larger gases (e.g., CO_2) than small gases (e.g., H_2), leading to significantly impaired size-sieving capability.

In recent years, polymeric membranes containing shape-persistent iptycene (i.e., triptycene and pentiptycene) moieties have been reported to exhibit promising separation performance in literature.[24-29] Iptycenes, including triptycene and pentiptycene, are a family of three-dimensional molecules with rigid and fused ring structures.[22, 30] Systematic studies on iptycene-based polyimides and polybenzoxazoles for gas separation membranes were reported by our group to elucidate the advantages of configurational free volume elements instilled by iptycene units.[31-36] For instance, the size-sieving nature of iptycene's internal free volume microporosity was able to maintain selectivity of triptycene-based polyimides after aging.[31-33] Moreover, backbone structures[34], substituent groups[31], and content of iptycene units[32] can be systematically varied, which enables comprehensive investigation of the fundamental structure-property relationship and provides versatile strategies to finely tune gas transport properties of iptycene-based polymers to meet various gas separation needs. Following these macromolecular design strategies, introducing permanent configurational free volume-based microporosity via the incorporation of shape-persistent structure units in PBI structures is expected to simultaneously improve H_2 permeability and maintain size-sieving capability at elevated temperatures. In our previous work, triptycene units were incorporated into PBI structures and the obtained triptycene-based PBI (TPBI) exhibited ~13 times higher H_2 permeability than *m*-PBI at 150 ºC with promising H_2/CO_2

selectivity (~6.8). Moreover, after doping with phosphoric acid, the acid doped/crosslinked TPBI showed further enhancement of H_2/CO_2 selectivity by ~135% due to tightened chain packing.[23] The promising separation performance of TPBI-based membranes indicated the great potential of the strategy of configurational free volume in macromolecular design for high-temperature H_2/CO_2 separations.

In this paper, we report a new pentiptycene-based polybenzimidazole (PPBI) with highly promising high temperature H_2/CO_2 separation performance, where bulkier and shape-persistent pentiptycene units with large fraction of configuration free volume are introduced into PBI structures via polycondensation of 3,3'diaminobenzidine and a pentiptycene-based dicarboxylic acid monomer. Systematic studies have examined how configurational free volume contributes to enhanced gas permeability as well as size-sieving property at elevated temperatures. To further tailor the polymer chain packing and improve size-sieving ability, acid doping using phosphoric acid (PA) or trans-aconitic acid (TaA) is applied to crosslink PPBI chains via proton transfer and hydrogen bonding (**Fig. 1**). The membrane properties and fundamental gas transport properties of the acid-doped films are comprehensively studied to investigate how different types of acid molecules would influence H_2/CO_2 separation performance at high temperatures.

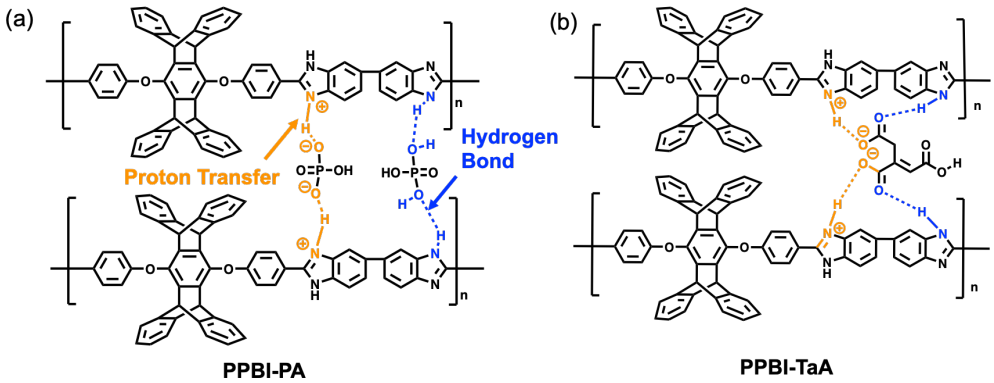

Fig. 1. Chemical structures of crosslinked PPBI by (a) phosphoric acid (PA) and (b) trans-aconitic acid (TaA). The proton transfer and hydrogen bonding interaction were labeled using orange and blue color respectively.

2. Materials and methods

2.1. Materials

Anthracene (TCI, >97%), *p*-benzoquinone (Sigma-Aldrich, ≥ 98%), 4-nitrobenzonitrile (TCI, >98%), potassium hydroxide (VWR), anhydrous sodium bicarbonate (Sigma-Aldrich, ≥99.7%), sodium hydrosulfite (Sigma-Aldrich, technical grade), hydrochloric acid (HCl, Sigma-Aldrich, 37%), acetic acid (EMD, ≥99.7%), xylenes (Sigma-Aldrich, ≥75%), anhydrous N,N-dimethylformamide (DMF, Sigma-Aldrich, ≥99.8%), toluene (VWR, ≥99.5), dimethyl sulfoxide (DMSO, Sigma-Aldrich, ≥99.9%), acetonitrile (VWR, ≥99.5%), ammonium hydroxide solution (VWR, 28-30%), N,N-dimethylacetamide (DMAc, BeanTown Chemical, ≥99%), phosphoric acid (Thermo Scientific, pure), trans-aconitic acid (Thermo Scientific, 98%), and Eaton's reagent (Sigma-Aldrich) were purchased and used as received. 3,3'-Diaminobenzidine (DAB, ≥99%) was purchased from BeanTown Chemical and was dried at 60 °C under vacuum before use.

2.2. Synthesis of pentiptycene-based dicarboxylic acid monomer (PPD)

Synthesis of pentiptycene-based dicarboxylic acid monomer (PPD) is shown in **Scheme 1** that was modified from the synthesis routes reported previously for triptycene-containing dicarboxylic acid monomer (TPD) and pentiptycene-based dianhydride monomer (PPDAn).[37, 38] A typical synthesis process is provided as follows: pentiptycene diol (Pent-OH) was firstly synthesized following the previously reported procedures mentioned above. To synthesize the pentiptycene-based dinitrile intermediate (Pent-2CN), Pent-OH (5.0 g, 10.8 mmol) and anhydrous potassium carbonate (K_2CO_3, 3.1 g, 22.2 mmol), toluene (9 mL), and anhydrous DMF (42 mL) were added in a 250 mL two-neck round-bottom flask connected with a N_2 flow adaptor and a Dean-Stark trap. The reaction mixture was refluxed at 120 °C for 3 h to deprotonate Pent-OH and

remove water as an azeotrope with toluene. After that, the mixture was cooled down to room temperature and 4-nitrobenzonitrile (3.3 g, 22.2 mmol) was added and the mixture was stirred at 100 ºC overnight. The crude pent-2CN was obtained by precipitating the mixture in a water/methanol (v/v=1/1, 600 mL) mixture. Crude Pent-2CN was further purified by refluxing in excessive acetonitrile (400 mL) at 80 ºC for 24 h. The high-purity and white Pent-2CN powder product (6.0 g, 83% yield) was filtered and dried at 100 ºC under vacuum.

To obtain pentiptycene-based dicarboxylic acid (PPD) monomer, Pent-2CN (2.0 g, 3.0 mmol) was hydrolyzed using potassium hydroxide (KOH, 18.0 g, 3.2 mol) in a DMSO/water mixture (80:80 mL/mL) for 48 h at 130 ºC. Upon the completion of the reaction, a clear solution containing deprotonated PPD product was obtained. The resulting clear solution was acidized to pH=1.0 using 6M HCl solution and the protonated PPD monomer was precipitated upon the acid addition, after which the final monomer, PPD (1.9 g, 90% yield), was collected via filtration and was dried at 100 ºC under vacuum overnight. ^{1}H NMR (400 MHz, DMSO-d_6): δ 5.53 (s, 4H), 6.80-6.82 (d, 4H), 6.90-6.92 (m, 8H), 7.11-7.14 (m, 8H), 7.96-7.96 (d, 4H), 12.92 (s, 2H). ^{1}H NMR spectra of Pent-2CN and PPD are included in **Fig. S1**.

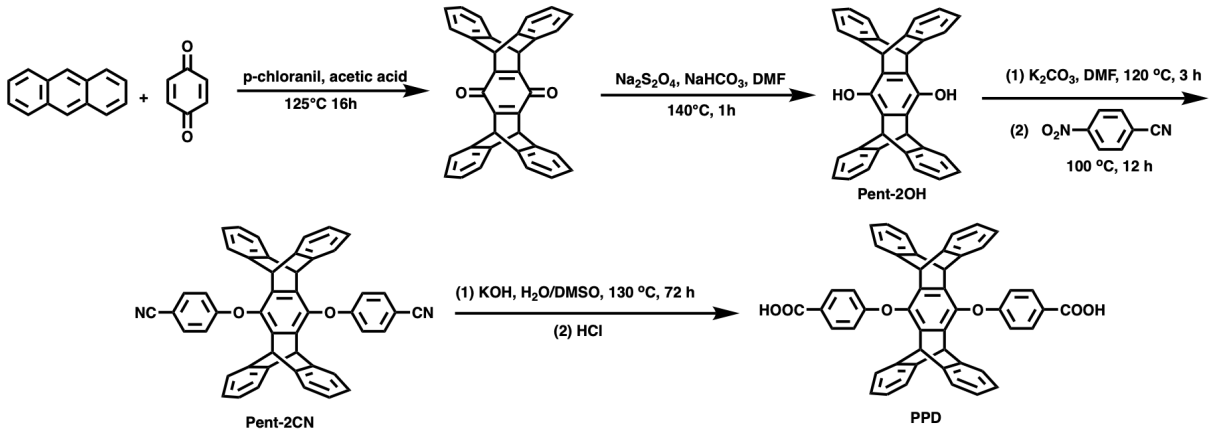

Scheme 1. Synthesis of pentiptycene-based dicarboxylic acid (PPD) monomer.

2.3. Synthesis of pentiptycene-based polybenzimidazole (PPBI)

The obtained PPD was polymerized with a commercially available tetraamine, DAB, via condensation polymerization to generate pentiptycene-based polybenzimidazole (PPBI) as shown in **Scheme 2**. The polymerization procedure is listed as follows: DAB (0.1540 g, 0.7 mmol) was added into a 100 mL round-bottom 3-neck flask and dissolved in Eaton's reagent (4.0 mL) at 80 ºC. Then, a stoichiometric amount of PPD (0.5 g, 0.7 mmol) was added along with additional Eaton's reagent (4.0 mL) to reach a total solid content of 8.0% (wt/vol). The mixture was then immersed in a pre-heated oil bath at 140 ºC. Upon the rapid dissolution of PPD, the viscosity of the reaction solution increased significantly. The reaction was terminated after about 16 min by pouring the solution into deionized (DI) water (600 mL) containing ammonium hydroxide solution (30 mL). This reaction time was established to balance high molecular weight and good solubility of PPBI product because PPBI obtained from a batch with longer reaction time couldn't be dissolved in DMAc solvent and thus couldn't be used for film preparation. Fibrous polymer product, PPBI, was obtained and was collected by filtration. The obtained solid was further washed in DI water (1000 mL) three times to remove residual solvents and salts, then was dried in a vacuum oven at 160 ºC overnight affording a brown fibrous solid as the final PPBI (0.6 g, 92% yield).

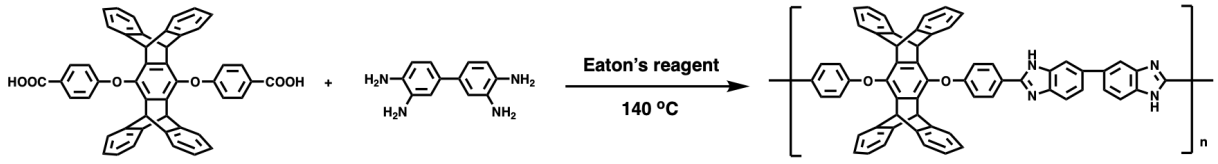

Scheme 2. Synthesis of pentiptycene-based polybenzimidazole (PPBI).

2.4. Preparation of PPBI thin films

Dense PPBI thin films were obtained via the solution casting method. A typical process is as follows: 0.25 g PPBI was dissolved in 4 mL DMAc and filtered with a 0.45 μm PTFE syringe

filter to remove insoluble particles and dust. After that, the clear filtered solution was cast onto a leveled and clean glass plate (1.5 in W × 3 in L) inside a vacuum oven. The temperature was set at 60 ºC overnight to slowly remove DMAc solvent under vacuum. The obtained transparent dense film was peeled off using a sharp blade, and further dried at 160 ºC under vacuum to remove residual solvent. After that, the film was washed in hot water (80 ºC) overnight and was further dried at 180 ºC. All final films were free of solvent, which was verified using proton nuclear magnetic resonance (^{1}H NMR) spectroscopy and thermogravimetric analysis (TGA).

The acid-doped PPBI films were prepared by immersing the PPBI films (~60 μm) in methanol solutions containing predetermined amounts of phosphoric acid (PA) or trans-aconitic acid (TaA). The film was stirred in methanol-acid solution for an extended period of time (i.e., 48 h for PA or 72 h for TaA) and then dried in a vacuum oven at 110 ºC overnight. The films after acid doping are named PPBI-PA and PPBI-TaA to indicate the type of acid used. The weights before and acid doping were measured as m_0 and m_1, respectively, and the doping level, *x*, was calculated using following equation (1), where M_{Acid} is the molecular weight of the acid and M_{PPBI} is the molecular weight of the repeat unit of PPBI:

$$x = \frac{\frac{m_1 - m_0}{M_{Acid}}}{\frac{m_0}{M_{PPBI}}} \quad (1)$$

2.5. Characterization

Chemical structures of PPD monomer and PPBI polymer were verified using ^{1}H NMR (proton nuclear magnetic resonance spectroscopy) on a Bruker AVANCE III HD 400 MHz spectrometer using deuterated sulfoxide (DMSO-d_6) and deuterated chloroform ($CDCl_3$) as a solvent.

Attenuated total reflection Fourier transform infrared spectroscopy (ATR-FTIR) was performed for PPBI polymer powder and dense films using a Bruker Tenor 27 FTIR instrument with a resolution of 4 cm^{-1} and 64 scans.

X-ray photoelectron spectroscopy (XPS, PHI VersaProb II) was performed on the pristine and acid-doped PPBI films (X-ray beam size:100 μm, powder: 100 W, and e-beam energy: 15 kV), and the pass energy was set to 23.5 eV with 15 sweeps. The obtained binding energy spectra of N 1s were fitted using Multipack software with the C-C bond as the reference to investigate the interactions between imidazole moieties and acid molecules.

Scanning electron microscopy (SEM) was carried out using the Thermo Prisma Environmental-SEM instrument (low vacuum mode) with energy dispersive spectrometry (EDS) to examine the acid doping efficiency.

Thermal properties of PPBI were investigated via thermal gravimetric analysis (TGA) under a constant nitrogen flow (50 mL/min) using a TGA Q500 instrument (TA Instruments) at a heating rate of 10 ºC/min. All samples were dried at 180 ºC in vacuum for 12 h before tests, and they were pretreated at 150 ºC for 30 min in the TGA instrument to remove absorbed water or residual solvent. Differential scanning calorimetry (DSC) analyses were carried out on a DSC QA2000 calorimeter (TA instruments). The first heating cycle was performed from room temperature to 400 ºC; the second heating cycle was from 100 ºC to 450 ºC with a heating rate of 10 ºC/min.

To investigate polymer chain packing of PPBI, wide-angle X-ray scattering (WAXS) was performed on an Aeries Benchtop X-ray diffractometer (Malvern Panalytical) with Cu Kα radiation source (wavelength λ=1.54 Å) at room temperature. The step size and scan speed were 0.02º per step and 0.4 s per step, respectively. The *d*-spacing values were then calculated from Bragg's law:

$$d = \frac{n\lambda}{2sin\theta} \quad (2)$$

The buoyancy method was used to measure the dry film density using a density kit of an analytical balance (ML204, Mettler Toledo) at room temperature. Cyclohexane was chosen as the medium due to the negligible solvent uptake for PPBI films. Density for each film was measured for at least six times and the average value was taken to estimate the fractional free volume (FFV) using the following equation:

$$FFV = \frac{V - V_o}{V_o} \quad (3)$$

$$V_o = 1.3 \times \sum V_W \quad (4)$$

V is the specific volume calculated from dry film density. V_o is the occupied volume estimated from theoretical van der Waals volume V_W calculated based on Bondi's group contribution method.

2.6. Gas permeability measurement

Pure-gas permeability values of PPBI and acid-doped PPBI film samples were measured using ultra-high-purity (UHP) gases (H_2 and CO_2) at various temperatures (35, 75, 100, 150, or 180 ºC) and in a broad pressure range (13-180 psig) via the constant-volume variable-pressure method. The samples were prepared by masking the film samples on to a brass disk with a pre-punched hole using Devcon 5-Minute Epoxy in Dual Syringe Tube. The permeable testing area was measured using a digital scanner with ImageJ analysis. The sample was loaded and degassed in the gas cell on both sides for at least 12 h. Before the permeation tests, the leak rate of the gas cell was recorded for at least 1 h. The steady state permeabilities of gas A, P_A, in Barrer (1 Barrer = 10^{-10} cm^3 (STP) cm/cm^2 s cm Hg) were obtained by monitoring the increase of downstream pressure and calculated using the following equation:

$$P_A = \frac{V_d l}{p_2 ART}\left[\left(\frac{dp_1}{dt}\right)_{ss} - \left(\frac{dp_1}{dt}\right)_{leak}\right] \quad (5)$$

where V_d is the fixed downstream volume of the gas cell in cm^3, l is the thickness of the films measured using a digital micrometer in cm, p_2 is the absolute upstream pressure in cm Hg, $\left(\frac{dp_1}{dt}\right)_{ss}$ and $\left(\frac{dp_1}{dt}\right)_{leak}$ are the rates of pressure increase (cm Hg/s) in the fixed downstream volume under steady-state and vacuum, respectively, A is the permeable testing area of the film sample in cm^2, R is the gas constant ($R = 0.278$ cm^3 cm Hg/cm^3 (STP)·K), and T is the measurement temperature (35, 75, 100, 150 or 180 °C). The H_2/CO_2 ideal selectivity was defined as the pure-gas permeability ratio of two gases (*i.e.*, H_2 and CO_2):

$$\alpha(A/B) = \frac{P_{H_2}}{P_{CO_2}} \quad (6)$$

The diffusion coefficient (D) of CO_2 was determined via the time-lag method using the following equation:

$$D = \frac{l^2}{6\theta} \quad (7)$$

in which θ is the lag time. The solubility coefficient (S) of CO_2 was calculated based on the obtained permeability and diffusivity values through the solution-diffusion theory:

$$S = \frac{P}{D} \quad (8)$$

Mixed-gas permeation tests were performed on a home-built gas permeation apparatus equipped with a gas chromatograph (GC) connected to the downstream pipeline. The 50:50 mol% H_2/CO_2 binary mixture was used with the feed pressure of 130 psig at 50-180 °C using argon as sweep gas and carrier gas. The composition of permeated gas mixture was analyzed by GC, and the mixed-gas permeability values in Barrer were determined based on the following equation:

$$P_A = 3223.7 \frac{x_{1A} S_F l}{x_{Ar}^P A(p_2 x_{2A} - p_1 x_{1A})} \quad (9)$$

where x_{1A} and x_{Ar}^P are the mole fractions of gas A (H_2 or CO_2) and argon in the permeate stream, respectively; x_{2A} is the mole fraction of gas A in the feed stream; S_F is the sweep gas flowrate (cm^3 (STP)/min), l is film thickness in μm; p_2 is upstream absolute pressure (psi), A is gas transport film area in cm^2. The mixed-gas selectivity values were calculated using the following equation:

$$\alpha(A/B) = \frac{\frac{x_{1A}}{x_{1B}}}{\frac{x_{2A}}{x_{2B}}} \quad (10)$$

in which x_{1A} and x_{1B} are the mole fractions of gas A and gas B in the permeate stream, respectively, while x_{2A} and x_{2B} are the mole fractions of component A and component B in the feeding stream.

3. Results and discussion

3.1. Synthesis and characterization of PPBI

The reaction temperature for polycondensation between DAB and pentiptycene-based dicarboxylic acid monomers was set at 140 °C to promote the cyclization of imidazole ring structures. During the polymerization, the viscosity of the reaction mixture increased significantly in a short period of time. To void the formation of insoluble gels reported in previous literature,[23, 39] an optimal reaction time was determined to be ~16-20 min, which produced high molecular weight polymers without gelation. Chemical structure of the obtained PPBI was confirmed by ^{1}H NMR and ATR-FTIR. As shown in **Fig. 2**, the presence of the peaks of aromatic protons (peaks h, i, and j) in the DAB unit and the characteristic peak of pentiptycene bridgehead (peak g)

demonstrated the successful incorporation of pentiptycene units.[32, 40] The broad and weak peak at about 13 ppm could be ascribed to the proton of N-H in imidazole rings, which may exchange with the deuterated solvent or absorbed water. In the ATR-FTIR spectrum, characteristic bands of C=C/C=N stretching (~1606 cm^{-1}), ring vibration of conjugation between benzene and imidazole rings (~1460-1492 cm^{-1}), self-associated N-H stretching (the broad band at ~3145 cm^{-1}), and non-hydrogen-bonded N-H stretching (~3302-3420 cm^{-1}) verify the benzimidazole structures.[41]

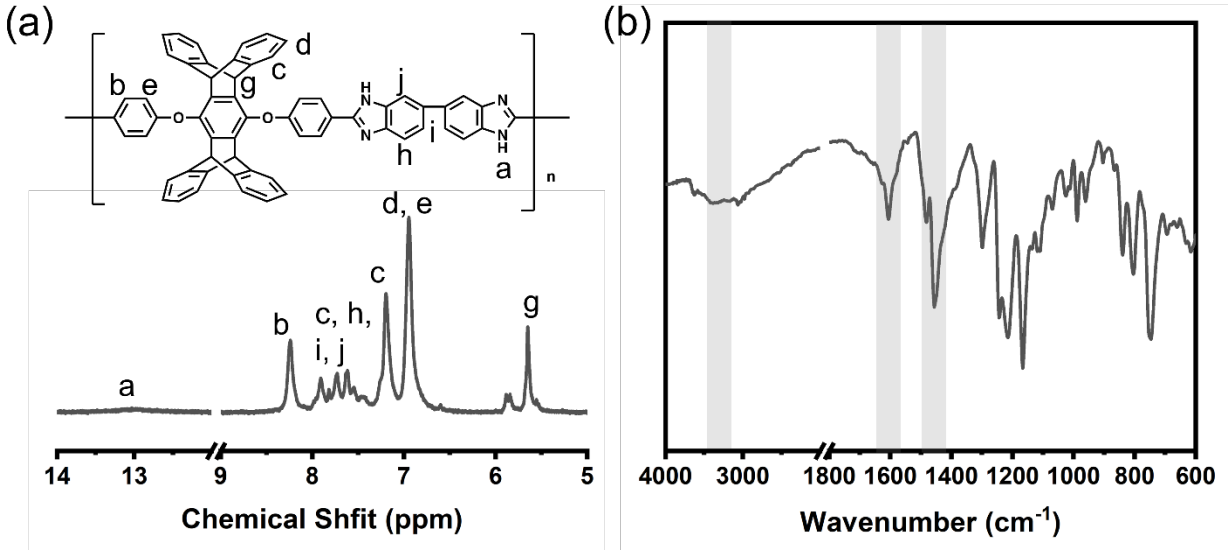

Fig. 2. (a) ^{1}HNMR spectrum and (b) ATR-FTIR spectrum of PPBI.

3.2. Fabrication and characterization of pristine and acid-doped PPBI films

Dense PPBI films were prepared via solution casting method, and the obtained robust films were crosslinked by doping with phosphoric acid (PA) or trans-aconitic acid (TaA) solution in methanol. The doping level values of the acid-doped films were calculated and listed in **Table S1**. As shown, PPBI-TaA exhibited a much lower acid doping level (0.40) than PPBI-PA (1.20), probably due to the bulkier size of TaA molecules limiting effective penetration into the dense PPBI films.

The ATR-FTIR spectra of pristine PPBI and acid-doped PPBI films in **Fig. 3a** verify the incorporation of acid molecules via the presence of the broad band O-H stretching of -COOH moieties at about 3100 cm^{-1}. The characteristic peaks of PO_2 (~1054 cm^{-1}) and $P(OH)_2$ (~837-931 cm^{-1}) indicate the formation of $H_2PO_4^-$ via proton transfer interaction with the imidazole moieties.[42, 43] PPBI-TaA film shows a small characteristic peak of C=O stretching (1710 cm^{-1}) that could be ascribed to unreacted carboxylic acid molecules.[37]

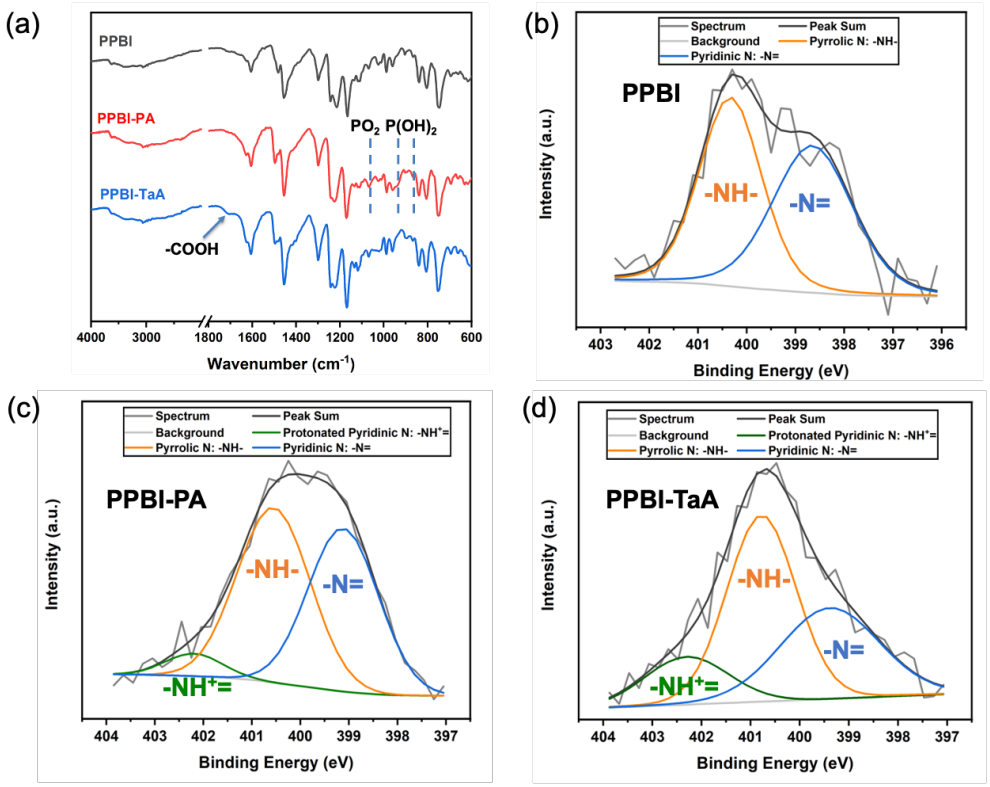

Fig. 3. (a) ATR-FTIR spectra of pristine PPBI and acid-doped PPBI films. (b) XPS N1s spectrum of pristine PPBI film. (c) XPS N1s spectrum of PPBI-PA. (d) XPS N1s spectrum of PPBI-TaA.

The surface and cross-section of acid-doped PPBI films were characterized using SEM with EDS mapping to analyze the distribution of acid molecules. As shown in **Figs. S2** and **S3**, phosphorus elements are distributed uniformly through the surface and cross-sectional areas,

indicating successful doping of phosphoric acid into PPBI films. Further, the surfaces of the two acid-doped films were characterized using XPS to investigate the interactions between acid and benzimidazole. Compared to as-cast pristine PPBI film, both acid-doped films display a new peak of protonated pyridinic N (i.e., -NH^+=), suggesting the proton transfer interactions between acid molecules and imidazole rings shown in **Fig. 3c** and **3d**.[44] Noticeably, the intensity of free pyridinic N (=N-) signals relative to that of pyrrolic N (-NH-) is significantly lower in the fitting profile of PPBI-TaA film. This is likely due to the relatively stronger acidity of TaA than PA, making TaA easier to protonate and ionically crosslink PBI chains.

Thermal properties of PPBI films were evaluated via TGA (**Fig. 4a**) and DSC (**Fig. S4**). No glass transition temperature was detected up to 450 ºC in DSC analysis of pristine PPBI polymer powder, and the as-cast pristine PPBI film does not show obvious weight loss below 480 ºC in TGA analysis, indicating its outstanding thermal stability and complete removal residual DMAc casting solvent. The thermal decomposition temperatures at 5% weight loss of pristine PPBI and acid-doped films are listed in **Table S1**. The PPBI-PA film exhibits a small weight loss at 200 ºC-300 ºC, which can be attributed to the release of water during the phosphoric acid-to-pyrophosphoric acid conversion. The TaA-doped film shows a lower degradation temperature ($T_{d,5\%}$ ~384 ºC) than PPBI and PPBI-PA, possibly due to the low decomposition temperature of TaA at ~150 ºC,[37] but it still demonstrated good thermal stability at the testing temperature range up to 180 ºC.

WAXS patterns of pristine and acid-doped PPBI films are compared with *m*-PBI film in **Fig. 4b** to investigate polymer chain packing affected by the incorporation of pentiptycene unit and acid doping. *d*-spacing values are calculated using Bragg's law and are listed in **Table S2**. Broad halos are observed in all films, indicating characteristic amorphous structures for

polybenzimidazole structures. As shown, all PPBI films show much larger *d*-spacing than *m*-PBI film due to the incorporation of bulk, shape-persistent pentiptycene units into polymer backbone, suggesting their much-improved gas permeability as discussed later. Compared to pristine PPBI film, the relative intensity of the peak associated with large *d*-spacing value (~7.7-8.0 Å) of the acid-doped PPBI films markedly reduced with the peak associated with small *d*-spacing value (~4.5-4.8 Å) became broader and shifted toward smaller *d*-spacing value, suggesting the formation of more densely packed structure induced by proton transfer and hydrogen bonding interactions in acid-doped films.

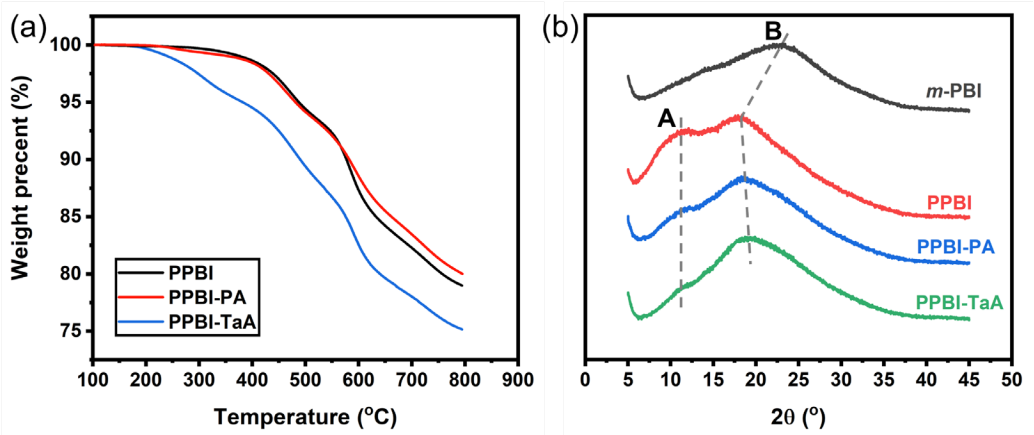

Fig. 4. (a) TGA curves of pristine PPBI and acid-doped PPBI films. (b) WAXD patterns of pristine PPBI and acid-doped PPBI films

3.3 Gas transport properties of pristine and acid-doped PPBI films

3.3.1 Effects of operating temperature on gas transport properties

Pure-gas separation performance of pristine PPBI and *m*-PBI films was evaluated at elevated temperature (35-180 °C) and 30 psig, and the full results are listed in **Table S3.** As shown in **Fig. 5a**, incorporating pentiptycene units resulted in significantly increased H_2 permeability by 40 times with expectedly reduced H_2/CO_2 selectivity at 35 °C due to the bulky structure of pentiptycene

units disrupting chain packing efficiently. With increasing testing temperature, H_2 permeability and H_2/CO_2 selectivity of PPBI enhanced simultaneously (**Fig. 5b**), resulting in much improved overall separation performance surpassing the upper bound. On the other hand, H_2/CO_2 selectivity of *m*-PBI decreased with increasing operating temperature. Specifically, H_2/CO_2 selectivity of PPBI increased by ~50%, while H_2/CO_2 selectivity of *m*-PBI decreases by ~25% with temperature increasing from 35 °C to 180 °C.

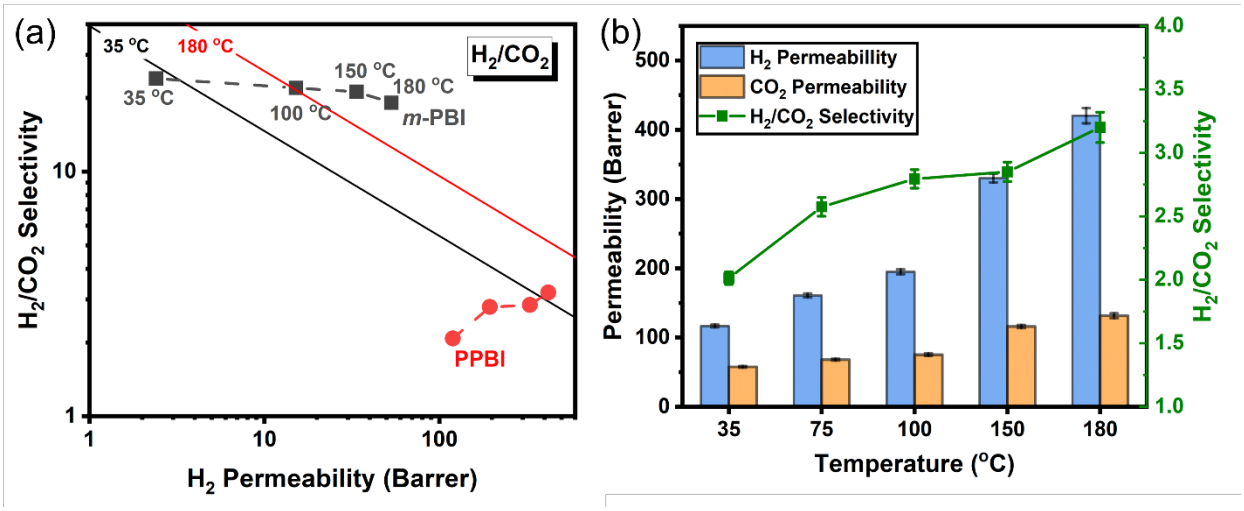

Fig. 5. (a) Comparison of overall separation performance of PPBI with *m*-PBI at various temperatures (35, 100, 150 and 180 °C). (b) Effects of testing temperature on H_2 permeability, CO_2 permeability, and H_2/CO_2 selectivity of PPBI. Permeability and selectivity were measured at 30 psig and 35-180 °C.

To further examine the temperature tolerance of PPBI containing configurational free volume, temperature dependence of permeability and selectivity data are fitted using Arrhenius-like equation. Activation energy of H_2 permeation (E_{p,H_2}) and activation energy CO_2 permeation (E_{p,CO_2}) are calculated using the slopes of fitted lines and tabulated in **Table S4**, and the E_{p,H_2} and E_{p,CO_2} data correspond well with previously reported data.[13, 14] As shown in **Fig. 6**, PPBI has much

lower activation energies of permeation than that of *m*-PBI, i.e., 5.2 kJ/mol *vs.* 24.4 kJ/mol for E_{p,CO_2} and 9.3 kJ/mol *vs.* 21.2 kJ/mol for E_{p,H_2}, in consistent with its much higher gas permeabilities due to its relatively loosely packed structure with incorporation of bulky pentiptycene units. For PPBI, its permeation activation energy for CO_2 (5.2 kJ/mol) is much lower than H_2 (E_{p,H_2} = 9.3 kJ/mol), which suggests that CO_2 permeability of PPBI increases much slower than H_2 permeability with increasing temperature, leading to increased overall H_2/CO_2 selectivity (**Fig. 6c**). Besides the expected effect of diminished CO_2 sorption at elevated temperatures, the stable configurational free volume elements instilled by pentiptycene units in PPBI play an important role in maintaining PPBI's size-sieving property and enhancing PPBI's high temperature tolerance than other glassy polymers, which experiencing significant selectivity loss at elevated temperatures.

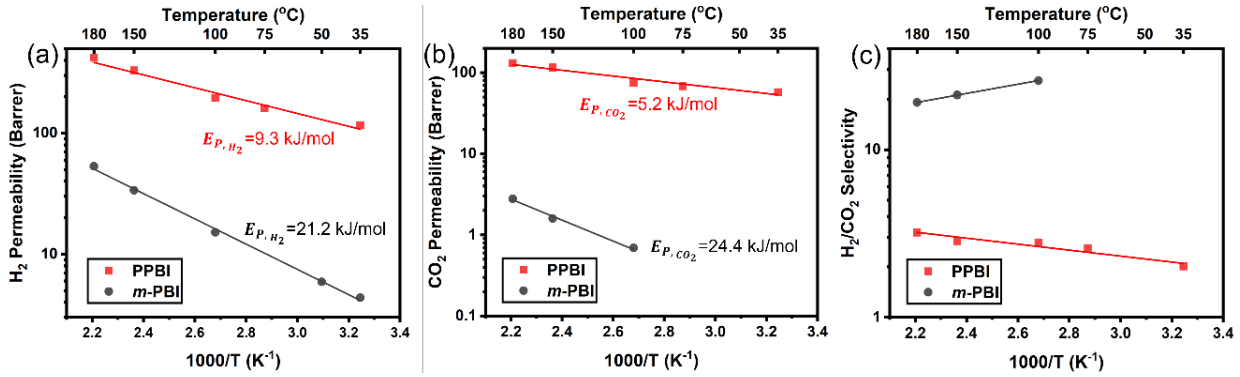

Fig. 6. Temperature dependence of (a) H_2 permeability, (b) CO_2 permeability, and (c) H_2/CO_2 selectivity of pristine PPBI and *m*-PBI.

Mixed-gas permeation tests were performed for pristine PPBI thin films at temperatures ranging from 50 to 180 °C using a H_2/CO_2 mixture (50/50 mol%) feed to match the typical composition of the gas mixtures for pre-combustion CO_2 capture from shifted syngas that contains about 55% H_2, 40% CO_2 and other gases, and the results are included in **Table S5** as well as plotted

in **Fig. 7**. Compared with the pure-gas permeation results, PPBI displayed lower permeabilities and higher H_2/CO_2 selectivity in the mixed-gas environment due to competitive sorption and a higher upstream pressure (130 psig) in mixed-gas permeation tests leading to saturation of sorption sites based on the dual-mode sorption theory.[45, 46] Competitive sorption between H_2 and CO_2 might also reduce the amount of available sorption sites, resulting in decreased permeability.[47, 48] Condensable gas, such as CO_2, is more sensitive to the change of available sorption sites. As such, the diminished CO_2 sorption with increasing temperature likely resulted in enhanced H_2/CO_2 selectivity at elevated temperatures.

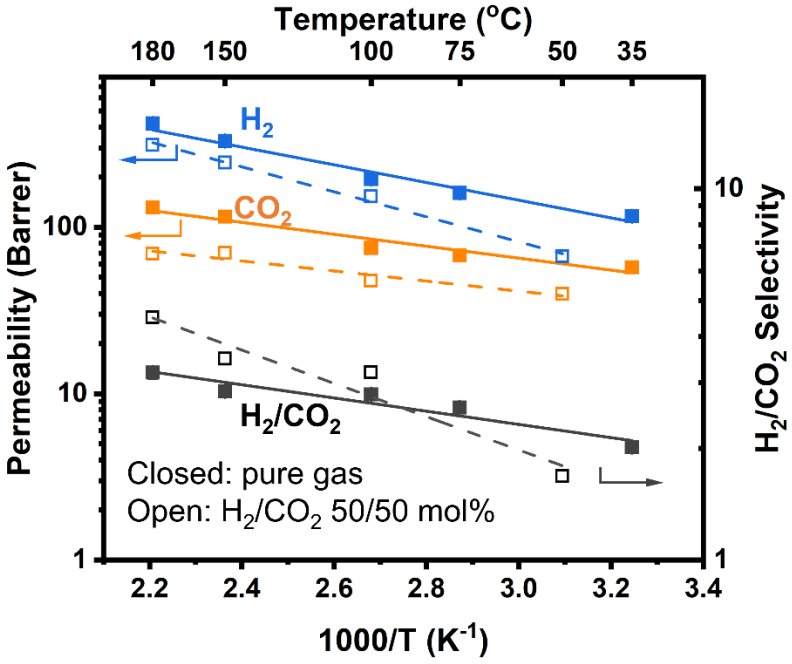

Fig. 7. Comparison of mixed-gas separation results with the pure-gas permeation results for pristine PPBI at 35-180 °C, 130 psig. (Open symbols represent 50:50 H_2/CO_2 mixed-gas permeation results and solid symbols are pure-gas results)

3.3.2 Effects of acid doping on PPBI separation performance

To further improve H_2/CO_2 selectivity, acid doping was applied on PPBI thin films using phosphoric acid (PA) and trans-aconitic acid (TaA) to facilitate acid crosslinking between imidazole moieties. Compared with PA, TaA has a relatively bulkier size which might be more effective to crosslink PPBI chains via proton transfer and hydrogen bonding considering the large interchain distance in PPBI. Additionally, TaA is a stronger acid than PA, and is more likely to protonate benzimidazoles rings more effectively by forming ionic crosslinked network structures.[37, 38] Pure-gas permeation tests of acid-doped PPBI films (i.e., PPBI-PA and PPBI-TaA) were conducted at elevated temperatures (35-180 ^oC) to investigate the effect of acid crosslinking on gas transport properties, of which the results are listed in **Table S3**. At ambient temperature (35 ^oC), acid-doped films exhibit significantly decreased H_2 and CO_2 permeability at 35 ^oC due to crosslinking-tightened chain packing via proton transfer and hydrogen bonding interactions between imidazole moieties and acid molecules (**Fig. S5a**), in consistent with WAXS results (**Fig. 4b**). As listed in **Table S3**, diffusivity and solubility coefficients of CO_2 were measured via the time-lag method at 13 psig following the solution-diffusion theory. H_2 diffusivity coefficients are not reported due to its very short lag time and large errors. At elevated temperatures, errors of calculated CO_2 diffusivity coefficients also increased significantly. Therefore, CO_2 diffusivity coefficients of pristine PPBI and acid-doped PPBI films measured at 35 ^oC are compared to investigate the effects of acid doping on separation performance. In general, the largely decreased permeability of acid-doped films at 35 ^oC can be attributed to drastic reduction of CO_2 diffusivity coefficients (**Fig. S5b**) due to the formation of densely packed structures upon acid crosslinking. The effect of acid doping on H_2/CO_2 selectivity shows a less straight forward trend when comparing the acid-doped films with pristine PPBI film at ambient conditions. Specifically, PPBI-PA film doped with phosphoric acid exhibited significantly improved H_2/CO_2 selectivity at 35 ^oC,

while PPBI-TaA film doped with bulkier trans-aconitic acid displayed similar H_2/CO_2 selectivity with that of pristine PPBI film. The different separation performance between two acid-doped films might be ascribed to their different doping level and corresponding crosslinking efficiency. Phosphoric acid, being relatively small in size, can penetrate into dense films more efficiently, resulting in more densely packed structures and consequently significant enhancement of H_2/CO_2 selectivity relative to undoped PPBI film. On the other hand, while doping PPBI with TaA also tightened chain pack as evidenced by greatly reduced H_2 and CO_2 diffusivity of PPBI-TaA film (**Fig. S5b**), TaA doping resulted in much enhanced CO_2 solubility than pristine PPBI and PPBI-PA films, resulting in higher CO_2 permeability and lower H_2/CO_2 selectivity than PPBI-PA film.

At elevated temperatures, the pristine and acid-doped PPBI films exhibited very different temperature tolerance when comparing their activation energies of permeation (E_p) shown in **Fig. 8** and tabulated in **Table S4**. Compared with pristine PPBI, acid-doped films exhibited much higher activation energies of permeation, in consistent with tightened chain packing due to acid doping. As shown in **Fig. 8b**, PPBI-PA shows the lowest CO_2 permeability at 35 ^oC, indicating the promising size-sieving property due to relatively higher doping level. However, CO_2 permeability of PPBI-PA increased much faster with increasing temperature as illustrated by its highest activation energy of CO_2 permeation. This observation might be ascribed to diminished hydrogen bonding at high temperatures, resulting in significant loss of size-sieving property. However, the decreased diffusivity selectivity of PPBI-PA seemed to be offset by the favored solubility selectivity at elevated temperatures. As a result, the overall H_2/CO_2 selectivity was relatively independent of temperature change for phosphoric acid doped PPBI-PA films (**Fig. 8c**). In contrast, PPBI films doped with TaA, i.e., PPBI-TaA, didn't show improved size-sieving property as expected, likely due to the relatively low acid doping level. However, it displayed more desirable

temperature dependence due to its relatively lower E_{p,CO_2}. CO_2 permeability of PPBI-TaA increased much slower with increasing temperature due to diminished CO_2 sorption and well-maintained size-sieving property. Therefore, the overall H_2/CO_2 selectivity of PPBI-TaA increased significantly at elevated temperatures (**Fig. 8c**), which is likely due to the relatively stronger acidity of TaA and the formation of ionically crosslinked network structure, as evidenced by XPS results. The ionically crosslinked network structure of PPBI-TaA is expected to limit chain relaxation more effectively and thus better maintain size-sieving property at high temperatures.

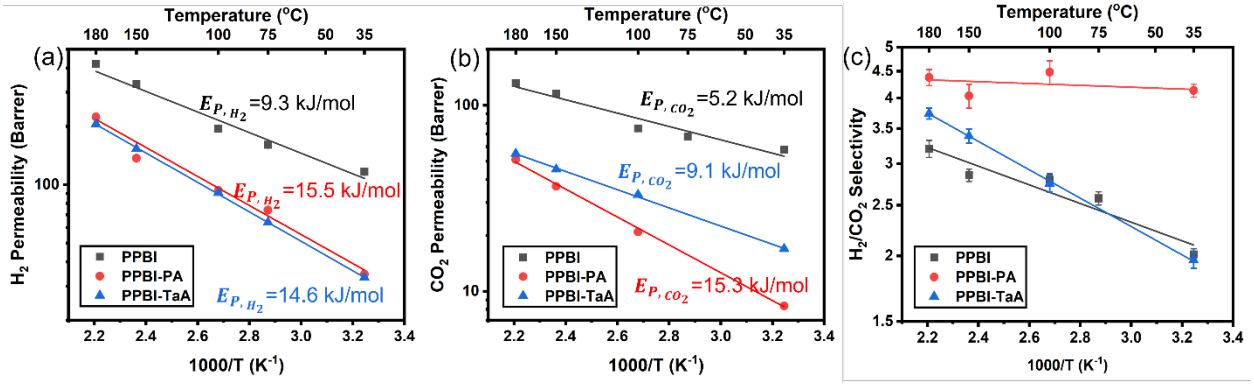

Fig. 8. Temperature dependence of (a) H_2 permeability, (b) CO_2 permeability, and (c) H_2/CO_2 selectivity of pristine PPBI and acid-doped PPBI films.

The overall separation performance of pristine PPBI film and acid-doped PPBI films under pure- or mixed-gas feed conditions is shown in **Fig. 9** and compared with the predicted H_2/CO_2 upper bound at 180 °C. As shown, acid-doped PPBIs displayed improved H_2/CO_2 selectivity with promising H_2 permeability at high temperatures as compared to pristine PPBI. Moreover, under mixed-gas feed conditions (50/50 mol% H_2/CO_2, 230 psig) at 180 °C, PPBI-TaA film showed significantly improved overall separation performance, approaching the predicted 180 °C upper bound. In **Fig. 9b**, the overall separation performance of pristine PPBI and acid-doped films are

compared in the upper bound plot with the predicted upper bound at 180 °C and state-of-the-art PBI-based membrane materials listed in **Table S6**. By incorporating bulky pentiptycene units, our novel PPBI membranes exhibit attractively high H_2 permeability and promising H_2/CO_2 selectivity, especially in the mixed gas environment, which demonstrates good temperature tolerance of stable configurational free volume elements.

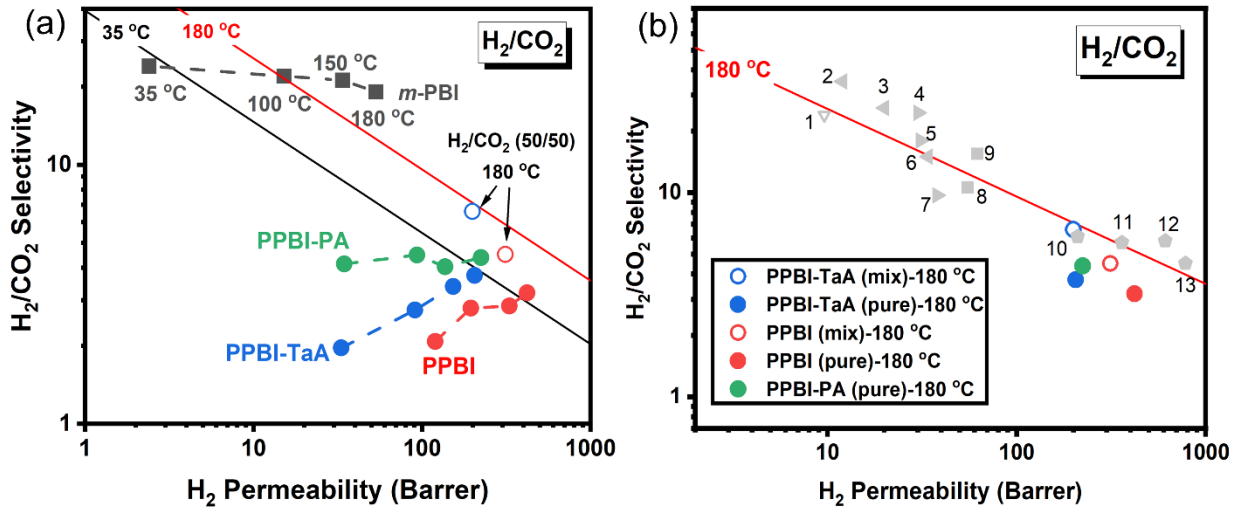

Fig. 9. (a) Overall separation performance of pristine and acid-doped PPBI films in pure-gas (solid symbols, 35-180 °C, 30 psig, **Table S3**) and mixed-gas environment (open circles, H_2/CO_2, 50/50 mol%, 180 °C, 230 psig, **Table S5**). (b) Comparison of the separation performance of pristine and acid-doped PPBI films at 180 °C with PBI-based membranes in literature. Sources of points 1-13 are tabulated in **Table S6**.

4. Conclusions

In this work, a novel pentiptycene-based polybenzimidazole, PPBI, has been successfully synthesized in high molecular weight and dense polymer films were fabricated. By incorporating shape-persistent pentiptycene units with intrinsic configurational free volume elements, PPBI

exhibited simultaneously enhanced H_2 permeability and H_2/CO_2 selectivity with increasing temperature. To further improve size-sieving property of PPBI films, H_3PO_4 and trans-aconitic acid molecules were introduced and crosslinked polymer chains via proton transfer and hydrogen bonding interactions. Compared with pristine PPBI, acid-doped films exhibited effectively improved H_2/CO_2 selectivity with promising H_2 permeability at high temperatures (up to 180 °C). Moreover, the temperature dependence of H_2/CO_2 selectivity was related with the type of acid. Specifically, TaA which has relatively higher acidity might protonate and ionically crosslink PPBI chains more effectively, leading to well-maintained size-sieving property at high temperatures. As the results, the diminished CO_2 sorption and well-maintained size-sieving property resulted in overall improved H_2/CO_2 selectivity with increasing temperature. All films including pristine PPBI and acid-doped PPBI displayed overall improved separation performance with increasing temperature, approaching the Robeson's upper bound estimated at 180 °C. demonstrating the great potential for high-temperature H_2/CO_2 separation.

CRediT authorship contribution statement

Mengdi Liu: Writing – original draft, Writing – review & editing, Visualization, Methodology, Investigation, Data curation. **Joseph Emory:** Writing – review & editing, Visualization, Methodology, Investigation. **Ruilan Guo:** Writing – review & editing, Funding acquisition, Conceptualization.

Declaration of competing interest

The authors declare that they have no known competing financial interests or personal relationships that could have appeared to influence the work reported in this paper.

Data availability

Data will be made available on request.

Acknowledgements

The authors acknowledge the financial support from the Division of Chemical Sciences, Biosciences, and Geosciences, Office of Basic Energy Sciences of the U.S. Department of Energy (DOE), under award no. DE-SC0024384. The authors thank the Center for Environmental Science and Technology (CEST) of the University of Notre Dame for the use of characterization facilities.

References

1. Sholl, D. S.; Lively, R. P., Seven chemical separations to change the world. *Nature* **2016,** *532* (7600), 435-437.

2. Sanders, D. F.; Smith, Z. P.; Guo, R.; Robeson, L. M.; McGrath, J. E.; Paul, D. R.; Freeman, B. D., Energy-efficient polymeric gas separation membranes for a sustainable future: A review. *Polymer* **2013,** *54* (18), 4729-4761.

3. Ockwig, N. W.; Nenoff, T. M., Membranes for Hydrogen Separation. *Chemical Reviews* **2007,** *107* (10), 4078-4110.

4. Shao, L.; Low, B. T.; Chung, T.-S.; Greenberg, A. R., Polymeric membranes for the hydrogen economy: contemporary approaches and prospects for the future. *Journal of Membrane Science* **2009,** *327* (1-2), 18-31.

5. Balzani, V.; Armaroli, N., *Energy for a sustainable world: from the oil age to a sun-powered future*. John Wiley & Sons: 2010.

6. Franz, J.; Scherer, V., An evaluation of CO2 and H2 selective polymeric membranes for CO2 separation in IGCC processes. *Journal of Membrane Science* **2010,** *359* (1-2), 173-183.

7. Galizia, M.; Chi, W. S.; Smith, Z. P.; Merkel, T. C.; Baker, R. W.; Freeman, B. D., 50th anniversary perspective: polymers and mixed matrix membranes for gas and vapor separation: a review and prospective opportunities. *Macromolecules* **2017,** *50* (20), 7809-7843.

8. Pesiri, D. R.; Jorgensen, B.; Dye, R. C., Thermal optimization of polybenzimidazole meniscus membranes for the separation of hydrogen, methane, and carbon dioxide. *Journal of Membrane Science* **2003,** *218* (1), 11-18.

9. O'Brien, K. C.; Krishnan, G.; Berchtold, K. A.; Blum, S.; Callahan, R.; Johnson, W.; Roberts, D.-L.; Steele, D.; Byard, D.; Figueroa, J., Towards a pilot-scale membrane system for pre-combustion CO_2 separation. *Energy Procedia* **2009,** *1* (1), 287-294.

10. Merkel, T. C.; Zhou, M.; Baker, R. W., Carbon dioxide capture with membranes at an IGCC power plant. *Journal of Membrane Science* **2012,** *389*, 441-450.

11. Miller, D. C.; Litynski, J. T.; Brickett, L. A.; Morreale, B. D., Toward transformational carbon capture systems. Wiley Online Library: 2016; Vol. 62, pp 2-10.

12. Jansen, D.; Gazzani, M.; Manzolini, G.; van Dijk, E.; Carbo, M., Pre-combustion CO2 capture. *International Journal of Greenhouse Gas Control* **2015,** *40*, 167-187.

13. Li, X.; Singh, R. P.; Dudeck, K. W.; Berchtold, K. A.; Benicewicz, B. C., Influence of polybenzimidazole main chain structure on H_2/CO_2 separation at elevated temperatures. *Journal of Membrane Science* **2014,** *461*, 59-68.

14. Stevens, K. A.; Moon, J. D.; Borjigin, H.; Liu, R.; Joseph, R. M.; Riffle, J. S.; Freeman, B. D., Influence of temperature on gas transport properties of tetraaminodiphenylsulfone (TADPS) based polybenzimidazoles. *Journal of Membrane Science* **2020,** *593*, 117427.

15. Borjigin, H.; Stevens, K. A.; Liu, R.; Moon, J. D.; Shaver, A. T.; Swinnea, S.; Freeman, B. D.; Riffle, J.; McGrath, J. E., Synthesis and characterization of polybenzimidazoles derived from tetraaminodiphenylsulfone for high temperature gas separation membranes. *Polymer* **2015,** *71*, 135-142.

16. Kumbharkar, S. C.; Kharul, U. K., Investigation of gas permeation properties of systematically modified polybenzimidazoles by N-substitution. *Journal of Membrane Science* **2010,** *357* (1), 134-142.

17. Kumbharkar, S. C.; Karadkar, P. B.; Kharul, U. K., Enhancement of gas permeation properties of polybenzimidazoles by systematic structure architecture. *Journal of Membrane Science* **2006,** *286* (1), 161-169.

18. Kumbharkar, S. C.; Kharul, U. K., New N-substituted ABPBI: Synthesis and evaluation of gas permeation properties. *Journal of Membrane Science* **2010,** *360* (1), 418-425.

19. Hosseini, S. S.; Teoh, M. M.; Chung, T. S., Hydrogen separation and purification in membranes of miscible polymer blends with interpenetration networks. *Polymer* **2008,** *49* (6), 1594-1603.

20. Naderi, A.; Asadi Tashvigh, A.; Chung, T.-S.; Weber, M.; Maletzko, C., Molecular design of double crosslinked sulfonated polyphenylsulfone /polybenzimidazole blend membranes for an efficient hydrogen purification. *Journal of Membrane Science* **2018,** *563*, 726-733.

21. Wang, L.; Guo, X.; Zhang, F.; Li, N., Blending and in situ thermally crosslinking of dual rigid polymers for anti-plasticized gas separation membranes. *Journal of Membrane Science* **2021,** *638*, 119668.

22. Corrado, T.; Guo, R., Macromolecular design strategies toward tailoring free volume in glassy polymers for high performance gas separation membranes. *Molecular Systems Design & Engineering* **2020,** *5* (1), 22-48.

23. Jiao, Y.; Liu, M.; Wu, Q.; Zheng, P.; Xu, W.; Ye, B.; Zhang, H.; Guo, R.; Luo, S., Finely tuning the microporosity in phosphoric acid doped triptycene-containing polybenzimidazole membranes for highly permselective helium and hydrogen recovery. *Journal of Membrane Science* **2023,** *672*, 121474.

24. Ghanem, B. S.; Swaidan, R.; Litwiller, E.; Pinnau, I., Ultra-microporous triptycene-based polyimide membranes for high-performance gas separation. *Advanced materials* **2014,** *26* (22), 3688-3692.

25. Mao, H.; Zhang, S., Synthesis, characterization, and gas transport properties of novel iptycene-based poly [bis (benzimidazobenzisoquinolinones)]. *Polymer* **2014,** *55* (1), 102-109.

26. Zhu, Z.; Zhu, J.; Li, J.; Ma, X., Enhanced Gas Separation Properties of Tröger's Base Polymer Membranes Derived from Pure Triptycene Diamine Regioisomers. *Macromolecules* **2020,** *53* (5), 1573-1584.

27. Ghanem, B. S.; Alghunaimi, F.; Wang, Y.; Genduso, G.; Pinnau, I., Synthesis of Highly Gas-Permeable Polyimides of Intrinsic Microporosity Derived from 1,3,6,8-Tetramethyl-2,7-diaminotriptycene. *ACS Omega* **2018,** *3* (9), 11874-11882.

28. Cho, Y. J.; Park, H. B., High Performance Polyimide with High Internal Free Volume Elements. *Macromolecular Rapid Communications* **2011,** *32* (7), 579-586.

29. Alghunaimi, F.; Ghanem, B.; Alaslai, N.; Swaidan, R.; Litwiller, E.; Pinnau, I., Gas permeation and physical aging properties of iptycene diamine-based microporous polyimides. *Journal of Membrane Science* **2015,** *490*, 321-327.

30. Weidman, J. R.; Guo, R., The Use of Iptycenes in Rational Macromolecular Design for Gas Separation Membrane Applications. *Industrial & Engineering Chemistry Research* **2017,** *56* (15), 4220-4236.

31. Wiegand, J. R.; Smith, Z. P.; Liu, Q.; Patterson, C. T.; Freeman, B. D.; Guo, R., Synthesis and characterization of triptycene-based polyimides with tunable high fractional free volume for gas separation membranes. *Journal of Materials Chemistry A* **2014,** *2* (33), 13309-13320.

32. Luo, S.; Liu, Q.; Zhang, B.; Wiegand, J. R.; Freeman, B. D.; Guo, R., Pentiptycene-based polyimides with hierarchically controlled molecular cavity architecture for efficient membrane gas separation. *Journal of Membrane Science* **2015,** *480*, 20-30.

33. Luo, S.; Wiegand, J. R.; Gao, P.; Doherty, C. M.; Hill, A. J.; Guo, R., Molecular origins of fast and selective gas transport in pentiptycene-containing polyimide membranes and their physical aging behavior. *Journal of Membrane Science* **2016,** *518*, 100-109.

34. Weidman, J. R.; Luo, S.; Breier, J. M.; Buckley, P.; Gao, P.; Guo, R., Triptycene-based copolyimides with tailored backbone rigidity for enhanced gas transport. *Polymer* **2017,** *126*, 314-323.

35. Weidman, J. R.; Luo, S.; Doherty, C. M.; Hill, A. J.; Gao, P.; Guo, R., Analysis of governing factors controlling gas transport through fresh and aged triptycene-based polyimide films. *Journal of Membrane Science* **2017,** *522*, 12-22.

36. Luo, S.; Zhang, Q.; Zhu, L.; Lin, H.; Kazanowska, B. A.; Doherty, C. M.; Hill, A. J.; Gao, P.; Guo, R., Highly Selective and Permeable Microporous Polymer Membranes for Hydrogen Purification and CO_2 Removal from Natural Gas. *Chemistry of Materials* **2018,** *30* (15), 5322-5332.

37. Hu, L.; Bui, V. T.; Huang, L.; Singh, R. P.; Lin, H., Facilely Cross-Linking Polybenzimidazole with Polycarboxylic Acids to Improve H_2/CO_2 Separation Performance. *ACS Applied Materials & Interfaces* **2021,** *13* (10), 12521-12530.

38. Pfendt, L.; Drazić, B.; Popović, G.; Drakulić, B.; Vitnik, Z.; Juranić, I., Determination of all pKa Values of Some di- and Tri-Carboxylic Unsaturated and Epoxy Acids and Their Polylinear Correlation with the Carboxylic Group Atomic Charges. *Journal of Chemical Research* **2003,** *2003* (5), 247-248.

39. Leykin, A. Y.; Fomenkov, A. I.; Galpern, E. G.; Stankevich, I. V.; Rusanov, A. L., Some aspects of polybenzimidazoles' synthesis in P_2O_5 containing condensation media. *Polymer* **2010,** *51* (18), 4053-4057.

40. Huang, Z.; Yin, C.; Corrado, T.; Li, S.; Zhang, Q.; Guo, R., Microporous Pentiptycene-Based Polymers with Heterocyclic Rings for High-Performance Gas Separation Membranes. *Chemistry of Materials* **2022,** *34* (6), 2730-2742.

41. Glipa, X.; Bonnet, B.; Mula, B.; Jones, D. J.; Rozière, J., Investigation of the conduction properties of phosphoric and sulfuric acid doped polybenzimidazole. *Journal of Materials Chemistry* **1999,** *9* (12), 3045-3049.

42. Zhu, L.; Swihart, M. T.; Lin, H., Unprecedented size-sieving ability in polybenzimidazole doped with polyprotic acids for membrane H_2/CO_2 separation. *Energy & Environmental Science* **2018,** *11* (1), 94-100.

43. Hu, L.; Bui, V. T.; Krishnamurthy, A.; Fan, S.; Guo, W.; Pal, S.; Chen, X.; Zhang, G.; Ding, Y.; Singh, R. P.; Lupion, M.; Lin, H., Tailoring sub-3.3 Å ultramicropores in advanced carbon molecular sieve membranes for blue hydrogen production. *Science Advances* **2022,** *8* (10), eabl8160.

44. Wu, J.; Chung, T.-S., Supramolecular Polymer Network Membranes with Molecular-Sieving Nanocavities for Efficient Pre-Combustion CO_2 Capture. *Small Methods* **2022,** *6* (1), 2101288.

45. Kanehashi, S.; Nagai, K., Analysis of dual-mode model parameters for gas sorption in glassy polymers. *Journal of Membrane Science* **2005,** *253* (1), 117-138.

46. Barrer, R. M., Diffusivities in glassy polymers for the dual mode sorption model. *Journal of Membrane Science* **1984,** *18*, 25-35.

47. Ricci, E.; Benedetti, F. M.; Dose, M. E.; De Angelis, M. G.; Freeman, B. D.; Paul, D. R., Competitive sorption in CO_2/CH_4 separations: the case of HAB-6FDA polyimide and its TR derivative and a general analysis of its impact on the selectivity of glassy polymers at multicomponent conditions. *Journal of Membrane Science* **2020,** *612*, 118374.

48. Genduso, G.; Ghanem, B. S.; Pinnau, I., Experimental mixed-gas permeability, sorption and diffusion of CO_2-CH_4 mixtures in 6FDA-mPDA polyimide membrane: unveiling the effect of competitive sorption on permeability selectivity. *Membranes* **2019,** *9* (1), 10.

Supporting Information

Microporous Pentiptycene-based Polybenzimidazole Membranes for High Temperature H_2/CO_2 Separation

Mengdi Liu, Joseph Emery, and Ruilan Guo

Department of Chemical and Biomolecular Engineering, University of Notre Dame

Indiana, 46556, United States

* Corresponding author. Email: rguo@nd.edu

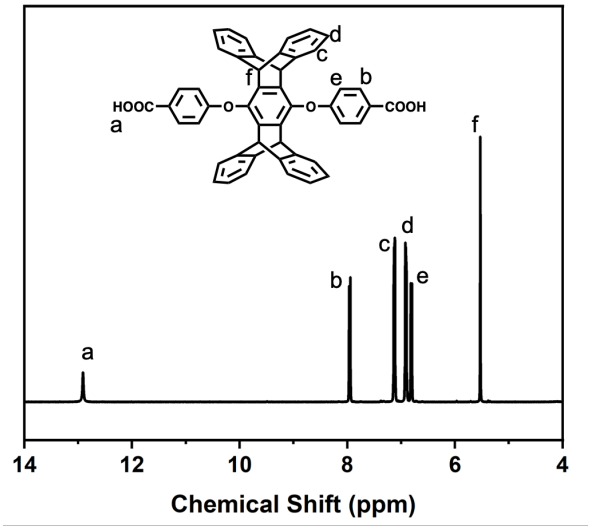

Fig. S1. ^{1}H NMR spectrum of pentiptycene-containing dicarboxylic acid (PPD) monomer.

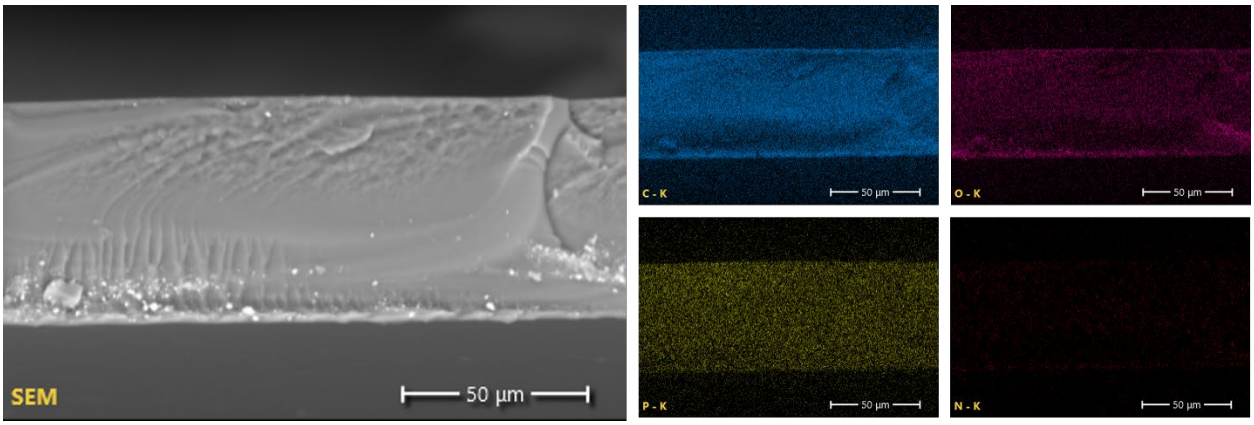

Fig. S2. SEM images of the cross-sectional area of PPBI-PA film with EDS mapping. Signals with different colors indicate C (blue), O (pink), P (yellow), and N (red), respectively.

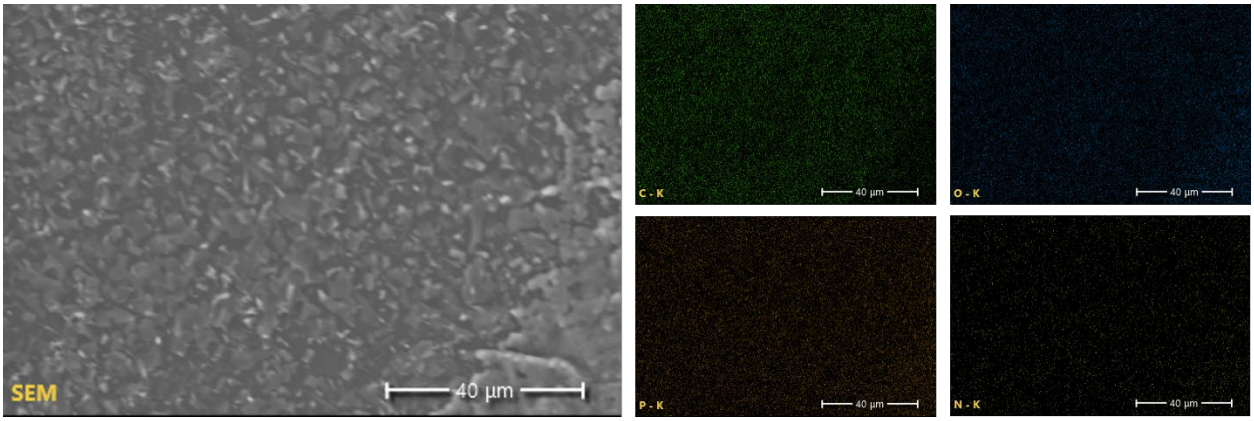

Fig. S3. SEM images of the surface area of PPBI-PA with EDS mapping. Signals with different colors indicate C (green), O (blue), P (orange), and N (yellow) respectively.

Table S1. Doping level, d-spacing values, and thermal properties of PPBI series

Sample	Acid concentration (g/mL)	Doping time (h)	Doping level	$T_{d,5\%}$ (°C)
PPBI	-	-	-	490.0
PPBI-PA	0.01	24	1.20	481.9
PPBI-TaA	0.03	48	0.40	384.2

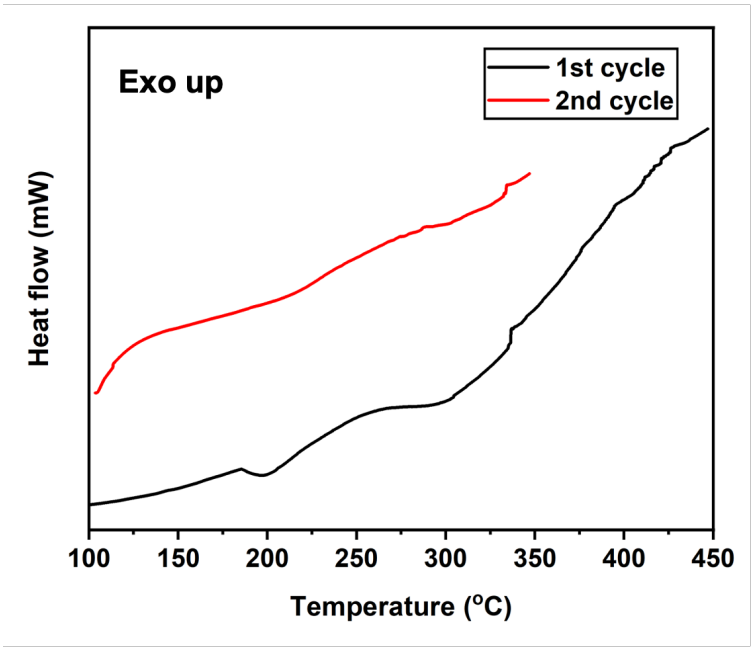

Fig. S4. DSC curves of pristine PPBI film. The endothermic bends in the first heating cycle could be ascribed to evaporation of absorbed water and residual solvent.

Table S2. Microstructure characteristics of pristine PPBI and acid-doped PPBI films

Sample	2θ (°)		*d*-spacing (Å)		Density (g/cm^3)	FFV (%)
	A	B	A	B		
m-PBI	-	23.1	-	3.8	1.352 ± 0.005	8.7
PPBI	11.0	19.9	8.0	4.5	1.253 ± 0.004	12.8
PPBI-PA	11.5	18.3	7.7	4.6	1.346± 0.006	9.2
PPBI-TaA	11.3	18.9	7.8	4.7	1.308 ± 0.005	10.3

Table S3. Pure-gas permeation results of *m*-PBI, PPBI, and acid-doped PPBI films

Sample	Temperature	Permeability (Barrer)[a]		H_2/CO_2 Selectivity	CO_2 Diffusivity D^b	CO_2 Solubility S^c
		H_2	CO_2			
m-PBI	100 ºC	14.2±0.3	0.7±0.03	22.0±1.2	-	-
	150 ºC	33.7±0.9	1.6±0.05	21.2±0.9	-	-
	180 ºC	53.2±1.2	2.8±0.08	19.1±0.7	-	-
PPBI	35 ºC	119.6±2.8	57.6±1.4	2.1±0.1	32.6±0.4	19.7±0.6
	75 ºC	160.6±2.9	62.4±1.4	2.6±0.1	51.8±4.2	13.1±1.1
	100 ºC	194.9±3.5	69.7±1.3	2.8±0.1	64.5±5.2	11.7±1.0
	150 ºC	330.2±6.2	115.7±2.2	2.9±0.1	234.7±28.1	5.3±0.6
	180 ºC	420.5±11.1	131.4±3.5	3.2±0.1	323.9±46.5	4.4±0.6
PPBI-PA	35 ºC	34.5±0.7	8.4±0.2	4.2±0.1	6.3±0.1	13.7±0.4
	100 ºC	93.4±3.8	20.8±0.6	4.5±0.2	18.0±0.6	11.8±0.8
	150 ºC	137.0±4.6	36.7±1.3	4.0±0.2	33.1±5.1	11.5±1.8
	180 ºC	224.0±5.0	51.1±1.4	4.4±0.2	81.2±15.9	7.1±1.4
PPBI-TaA	35 ºC	33.2±0.8	16.9±0.4	2.0±0.1	3.4±0.02	50.0±1.5
	100 ºC	90.7±2.2	33.0±0.9	2.7±0.1	10.0±0.9	34.9±3.3
	150 ºC	153.2±3.3	45.2±1.0	3.4±0.1	31.6±2.3	15.5±1.2
	180 ºC	205.4±3.3	54.9±0.9	3.7±0.1	60.7±8.4	9.7±1.4

NOTE:
[a] Permeability was measured at 30 psig
[b] Units: *D*, 10^{-9} cm^2/s; *S*, 10^{-2} cm^3(STP)/cm^3*cmHg. CO_2 diffusivity coefficients were measured at 13 psig and solubility coefficients were calculated using solution-diffusion theory. H_2 diffusivity coefficients were not shown due to a very short lag time.

Table S4. Activation energies of permeation of *m*-PBI, PPBI, and acid-doped PPBI films.

Sample	E_{P,H_2} (kJ/mol)	E_{P,CO_2} (kJ.mol)
m-PBI	21.2±1.2	24.4±2.0
PPBI	9.3±1.0	5.2±0.9
PPBI-PA	15.5±1.3	15.3±0.7
PPBI-TaA	14.6±0.1	9.1±0.6

Table S5. Mixed-gas permeation results of pristine PPBI films

Sample	Temperature	Permeability (Barrer)		H_2/CO_2 Selectivity
		H_2	CO_2	
PPBI	50 °C	62.6	39.7	1.7
	100 °C	153.1	47.8	3.2
	150 °C	244.7	70.1	3.5
	180 °C	312.5	69.4	4.5
PPBI-TaA	180 °C	199.3	31.2	6.6

NOTE: Mixed-gas permeability and selectivity were measured using the binary H_2/CO_2 50/50 mol% gas mixture at 130 psig.

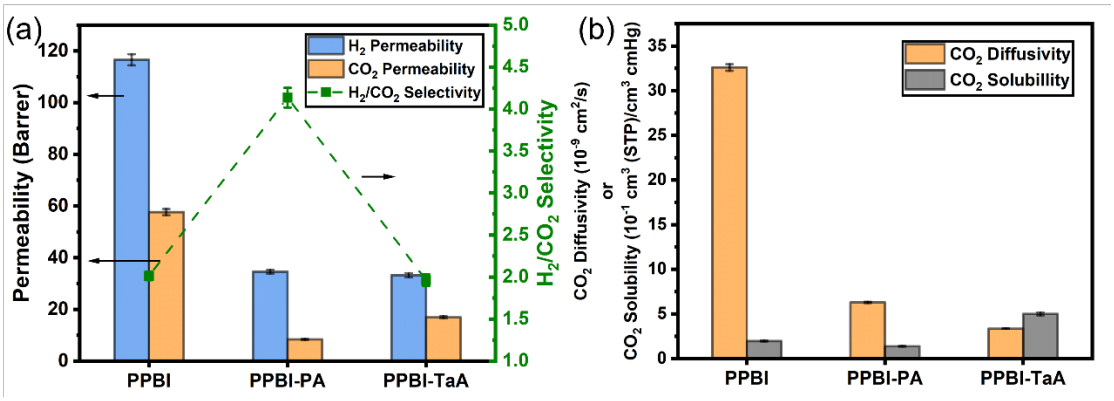

Fig. S5. (a) H_2 permeability, CO_2 permeability, and H_2/CO_2 selectivity (measured at 35 °C, 30 psig); (b) CO_2 diffusivity and CO_2 solubility coefficients (measured at 35 °C, 13 psig) of pristine PPBI, PPAI-PA, and PPBI-TaA.

Table S6. Separation performance of previously reported PBI-based membranes in literature as shown in **Fig. 9**.

#	Membrane	H_2 permeability (Barrer)	H_2/CO_2 selectivity	Temp. (^oC)	Feed pressure	Ref.
1	PBI-$TBB_{0.21}$-mix	9.6	24	150	14 atm	1
2	PBI-$(H_3PO_4)_{0.16}$	12	35	150	14 atm	2
3	PBI-$TaA_{0.2}$	20	26	150	14 atm	3
4	TADPS-IPA	30.1	24.6	190	3 atm	4
5	TADPS-TPA	31	18	190	3 atm	4
6	PBI-$OA_{0.16}$	34	15	150	14 atm	3
7	TADPS-OBA	38	9.7	190	3 atm	4
8	PBI-$PdT_{0.15}$	55	10.6	150	14 atm	5
9	PBI-$(Ni(TFA)_2)_{0.16}$	62	15.5	150	14 atm	5
10	PFCB-PBI	210	6.1	200	50 psi	6
11	Phenylidane-PBI	360	5.7	200	50 psi	6
12	BTBP-PBI	610	5.8	200	50 psi	6
13	6F-PBI	780	4.5	200	50psi	6

References

1. Naderi, A.; Asadi Tashvigh, A.; Chung, T.-S., H_2/CO_2 separation enhancement via chemical modification of polybenzimidazole nanostructure. *Journal of Membrane Science* **2019,** *572*, 343-349.

2. Zhu, L.; Swihart, M. T.; Lin, H., Unprecedented size-sieving ability in polybenzimidazole doped with polyprotic acids for membrane H_2/CO_2 separation. *Energy & Environmental Science* **2018,** *11* (1), 94-100.

3. Hu, L.; Bui, V. T.; Huang, L.; Singh, R. P.; Lin, H., Facilely Cross-Linking Polybenzimidazole with Polycarboxylic Acids to Improve H_2/CO_2 Separation Performance. *ACS Applied Materials & Interfaces* **2021,** *13* (10), 12521-12530.

4. Stevens, K. A.; Moon, J. D.; Borjigin, H.; Liu, R.; Joseph, R. M.; Riffle, J. S.; Freeman, B. D., Influence of temperature on gas transport properties of

tetraaminodiphenylsulfone (TADPS) based polybenzimidazoles. *Journal of Membrane Science* **2020,** *593*, 117427.

5. Hu, L.; Fan, S.; Huang, L.; Bui, V. T.; Tran, T.; Chen, K.; Ding, Y.; Swihart, M. T.; Lin, H., Supramolecular Polymer Networks of Ion-Coordinated Polybenzimidazole with Simultaneously Improved H_2 Permeability and H_2/CO_2 Selectivity. *Macromolecules* **2022,** *55* (15), 6901-6910.

6. Li, X.; Singh, R. P.; Dudeck, K. W.; Berchtold, K. A.; Benicewicz, B. C., Influence of polybenzimidazole main chain structure on H_2/CO_2 separation at elevated temperatures. *Journal of Membrane Science* **2014,** *461*, 59-68.